CONFERENCE PRE-PRINT

BREAKING OF THE ION TEMPERATURE SATURATION IN ELECTRON HEATED PLASMAS WITH TURBULENCE STABILIZATION

P. MANAS CEA, IRFM Saint-Paul-les-Durance, France Email: pierre.manas@cea.fr

¹P. MANAS, ²J. RUIZ RUIZ, ¹J. GARCIA, ¹J.F. ARTAUD, ¹C. BOURDELLE, ¹T. FONGHETTI, ³Y. KAZAKOV, ¹J. MORALES, ¹V. OSTUNI, ⁴J. CITRIN AND THE WEST TEAM*

¹CEA, IRFM, Saint-Paul-les-Durance, France

Abstract

The ion temperature saturation in plasmas of medium sized magnetic confinement machines has been consistently observed in regimes of dominant electron heating. This has raised concerns for future reactors as the fusion yield depends strongly on the achievable core ion temperature and that alpha heating predominantly heats the electrons. In the tokamak WEST these observations of ion temperature saturations have been explained by a competition between the ion-electron collisional heat-exchange and the energy confinement time. This trend is recovered with integrated modelling and provides insights for an ITER Q=10 scenario where this saturation is not found, due to higher energy confinement times and densities. Furthermore, there exists regimes where this saturation can be mitigated in dominant electron heated plasmas. This has been observed in W7-X but also in tokamaks, e.g. in WEST with nitrogen seeding and more strikingly on JET where a fast ion driven transport barrier is formed, following ICRH heating. The reasons for this reduced core T_i saturation are investigated with a range of plasma parameters from WEST to Tore Supra and JET including internal transport barriers formed at low (negative magnetic shear) and high densities (fast ions), with respectively, strong and weak ion-electron collisional coupling. Results from integrated modelling suggest that the ion central temperature breaking is obtained in particular conditions, consistent with experimental observations, that is, at high electron to ion heat diffusivities, high densities and reduced ion neoclassical heat diffusivities.

1. INTRODUCTION

The achievable central ion temperature is observed to be limited in current magnetic fusion machines (tokamaks [1,2] or stellarators [3]) in the case where electron heating is dominant. This raises questions on the achievable fusion performance of a future reactor since the fusion reaction rate from thermal deuterium and tritium fuel significantly depends on the ion temperature. Furthermore, highly energetic alpha particles will mainly drive electron heating, the fuel ions being heated only partly from these alphas and from collisional equipartition with thermal electrons, resulting in an overall dominant electron heating. To understand if this limitation in current machines is or can be alleviated in future machines, a WEST database is studied, where the central ion temperature saturation is observed. It is found that the central electron to ion temperature ratio directly correlates with global quantities, namely the global energy confinement time (τ_E) and the volume averaged electron-ion collisional heat exchange time (τ_{ei}) [2]. This correlation is recovered by the modelling using QLKNN-10D [6] in METIS [7] for turbulent transport and temperature profile predictions. It is then compared to a JET ICRH heated plasma [4] where the three-ion heating scheme is used [5] and MeV ions are generated, transferring their energy by more than 90% on the electron population. In the absence of a central Internal Transport Barrier (ITB), JET and WEST plasmas (and an ITER-like Q=10 scenario) follow the same global trend of decreasing central T_i/T_e with increasing τ_{ei}/τ_E . However, the global scaling is also shown to be broken in JET cases where a central ITB form due to turbulence stabilisation via fast ion driven modes [4]. In this case, higher central ion temperature can be achieved despite dominant central electron heating. Interestingly, similar observations have been found on W7-X with ITG turbulence stabilisation in pellet fuelled plasmas, concomitant to the formation of strong density gradients [8,9]. Following these evidences of central ion temperature saturation breaking in JET ICRH heated plasmas, additional data on WEST with nitrogen seeding [14] and on Tore Supra and JET featuring central ITBs with negative magnetic shear [10-13] have been added to the analysis. Further integrated modelling with ad-hoc central turbulence stabilisation has also been performed, based on these additional observations, and is used to

²Rudolf Peierls Centre for Theoretical Physics, University of Oxford, OX1 3NP, UK

³Laboratory for Plasma Physics, ERM/KMS, TEC Partner, 1000 Brussels, Belgium

⁴Google Deepmind, London, UK

^{*}see http://west.cea.fr/WESTteam

disentangle the main mechanisms responsible for alleviating the central ion temperature saturation in medium sized electron heated plasmas.

In Section 2, the context of this ion temperature saturation is recalled, with a particular emphasis on the WEST data together with refined integrated modelling frameworks and models used in a dynamical power scan at different plasma densities. In section 3, cases of ion temperature saturation breaking are discussed, including WEST nitrogen seeded scenarios and JET ICRH heated plasmas. In section 4, these experimental observations are complemented with cases featuring turbulence stabilisation, that is, Tore Supra and JET discharges with low densities and internal transport barriers triggered by a negative magnetic shear. Finally, integrated modelling, guided by these experimental evidences, is used to provide insights on the impact of central turbulence stabilisation, collisional heat exchange and ion to electron heat transport.

2. ION TEMPERATURE SATURATION IN WEST LHCD HEATED PLASMAS

The WEST database used in this work [2] consists of \sim 560 L-mode plasmas including plasma currents of 0.5 MA, magnetic field 3.7 T, line averaged densities ranging from 2.5 to 6 \times 10¹⁹ m⁻³ and LHCD injected power between 1 and 5.5 MW. The electron temperature is measured from Electron Cyclotron Emission, the ion temperature from the neutron rate (provided additional information on the plasma composition) and the electron

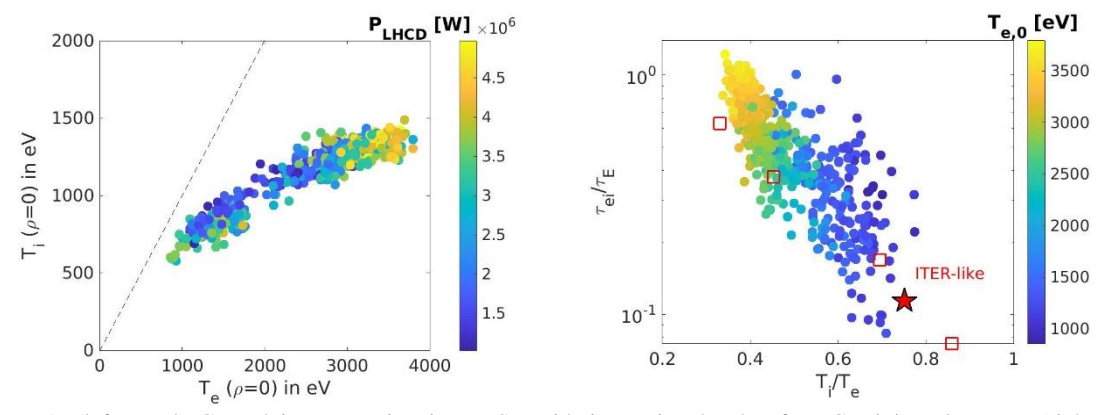


Figure 1: (left panel) Central ion saturation in WEST with increasing levels of LHCD injected power. (right panel) Competition between the collisional heat exchange time and the energy confinement time versus the core ion to electron temperature ratio. Integrated modelling results are also shown for WEST (red squares) and for a Q=10 ITER-like scenario (red star).

density from interferometry. Similar saturation of T_i as found in AUG and W7-X is observed around 1.5 keV (Fig. 1 left panel). Performing integrated modelling (METIS+QLKNN-10D) from a reference case and scanning the LHCD injected power from 1 to 3.8 MW results in quantitatively similar saturation. The role of the increased electron to ion temperature ratio in turbulence destabilisation has been investigated with QLKNN-10D and found to have limited impact on such achievable central T_i in this case. Due to the observed strong correlation between the T_i/T_e and the ratio of the two characteristic times τ_{ei}/τ_E (Fig. 1 right panel) in the modelling and experimental data, ways to improve the highest achievable central ion temperature are explored from simulations, either by

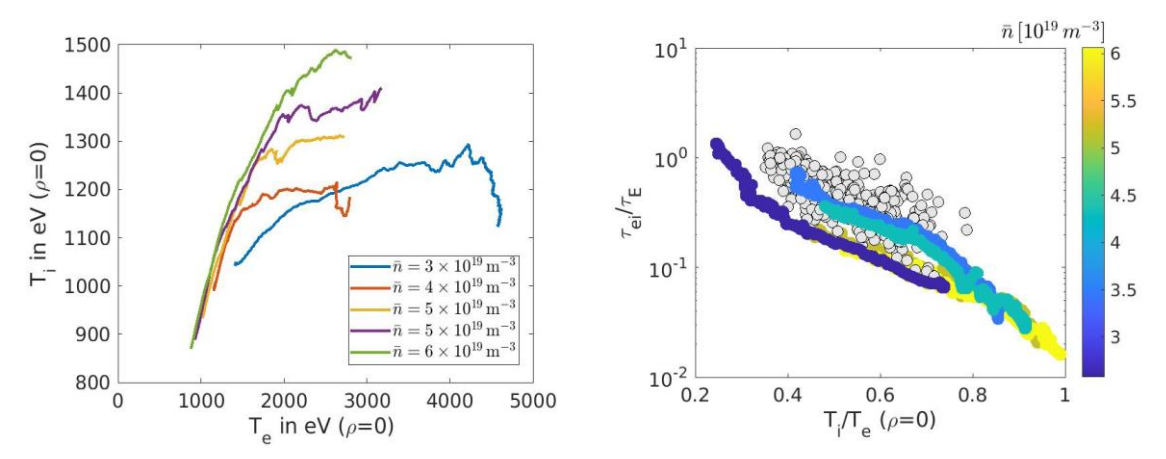


Figure 2: (left panel) LHCD power ramp-up in the HFPS with TGLF sat-2 and the LHCD power/current deposition reduced model. (right panel) Time traces of these simulations compared to experimental WEST data (gray circles). The ratio of the collisional heat exchange time and the energy confinement is used.

decreasing the volume averaged electron-ion collisional heat exchange time or by increasing the energy confinement time. Increasing the density allows to increase the collisional coupling between electrons and ions while also impacting the energy confinement time. This results in larger T_i/T_e at lower τ_{ei}/τ_E . These findings using steady state simulations with METIS/QLKNN-10D are also reproduced using the integrated modelling framework HFPS [17]. These simulations are shown in Fig. 2 where a LHCD power deposition model is used [15] together with TGLF-sat2 [14] for turbulent transport. Here the main differences come from the consistent source/transport models and the dynamical aspect, i.e. ramp in LHCD power are performed at different plasma densities resulting in time evolution of the central ion and electron temperatures. This supports previous integrated modelling work with simplifying assumptions (such as constant LHCD power deposition) and further highlights the increase in density to be one of the main knobs for alleviating the central ion temperature in electron heated plasmas. In a different way, it was also shown that increasing the machine size at constant aspect ratio, q_{95} , magnetic field and external power density, results in higher T_i/T_e ratios due to larger energy confinement times at higher major radius. This machine size dependent trend is further complemented with modelling of a Q=10 ITER-like scenario featuring high electron and ion central temperatures due to larger confinement times and densities.

3. CENTRAL ION TEMPERATURE SATURATION BREAKING IN WEST AND JET

3.1. NITROGEN SEEDING IN WEST

Since 2023, WEST has developed scenarios with partial detachment and the formation of a radiation front

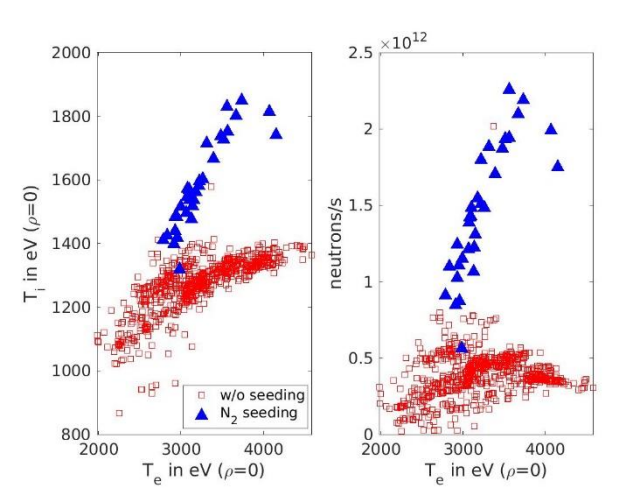
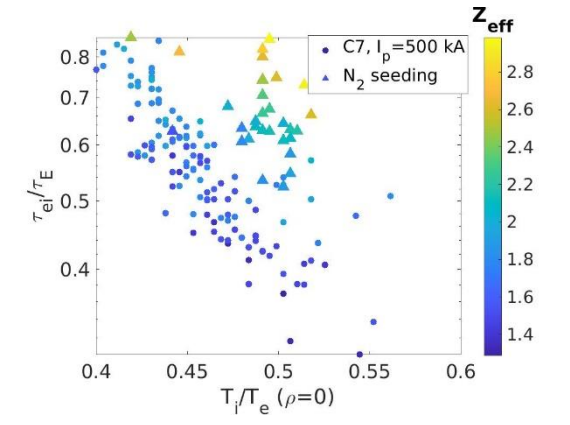


Figure 3: (left panel) Central ion temperature versus electron temperature for similar scenarios with and without nitrogen seeding. (right panel) The neutron rate is also shown.

localised in the X-point region, following nitrogen injections [14]. These scenarios presented improved performances in terms of central electron and ion temperatures, starting from the nitrogen injections. In Fig. 3 a reduced database including such scenarios is shown. It is clearly observed, from the increased neutron rate, that the ion temperature increase departs from the typical saturated value at such levels of central electron temperature. This is further shown with respect to τ_{ei}/τ_E in Fig. 4 and a clear breaking of the global trend is found with increasing levels of effective charge Z_{eff} . It has to be noted that the inclusion of the additional low Z species (N) does not change the collisional power exchange between ions and electrons due to the same mass over charge ratio as the main ions. Gradient-driven simulations have



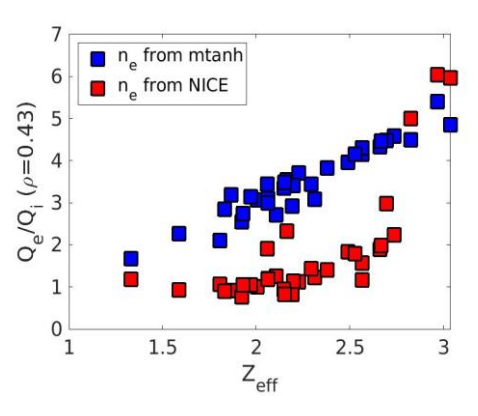


Figure 4: (left panel) Ion-electron collisional heat exchange over energy confinement time versus central ion to electron temperature ratio for a WEST database featuring nitrogen seeded scenarios (triangles). (right panel) Local electron to ion heat flux ratios computed with TGLF-sat2 for the same plasmas as shown in the left panel. For comparison, the electron density obtained from interferometry inversions using a modified hyperbolic tangent or an equilibrium reconstruction with the code NICE are shown.

been performed with TGLF-sat2 for these scenarios and the electron to ion heat flux is shown in Fig. 4 right panel at the normalised toroidal magnetic flux $\rho=0.43$. Despite the limit of such exercise, i.e. uncertainties on the local ion temperature gradients due to lack of direct localised measurements and on the electron density gradients (depending on interferometry inversion methods), a clear trend of increasing electron over ion heat flux is found with increasing effective charge. To bypass these limitations, a flux-driven integrated modelling effort on this dataset has been started and is currently ongoing [18]. Finally, the increase in core ion temperature is consistent with increased ITG stabilisation from main ion dilution as observed in other machines [19, 20]. The relative impact of such turbulence stabilisation on ion versus electron heat transport will be further discussed in section 5.

3.2. JET dominant electron heated plasmas with ICRH

Turning to a larger device, JET, discharge #97090, with dominant electron heating [4], features increase in the confinement factor and deep-core ion temperature in combination with the presence of unstable Alfvénic activity. This is an L-mode with a plasma current of $I_p = 2.4$ MA, toroidal magnetic field $B_0 = 3.2$ T and electron density of $n_e \sim 3.5 - 4 \times 10^{19} m^{-3}$ kept approximately constant throughout the discharge. The plasma includes phases with increasing ICRH power of $P_{ICRH} = 2$ MW (low), 4 MW (medium) and 7 MW (high). These phases correspond to the time windows t=9.2-10.9 s, t=11.3-13.4 s, and t=14-16 s respectively (Fig. 6). NBI blips are used for ion temperature measurements. A trace population of 3 He ions of density $n_{He}/n_e \sim 0.2$ -0.3 % was

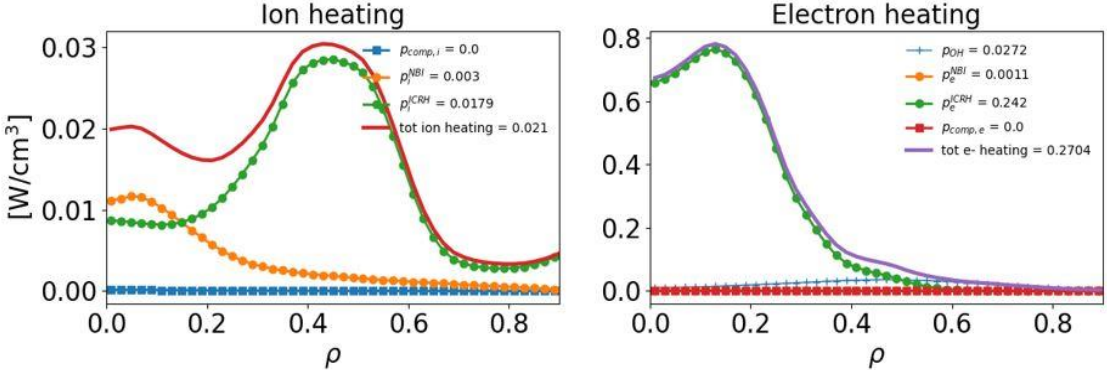


Figure 5: Ion and electron external power deposition for JET pulse #97090 during the highest ICRH phase. The total integrated power for each contribution, including the NBI power from blips and the total injected power, is given within the figures.

introduced into the plasma to absorb the ICRH power [5], and was accelerated to energies of $E(^3He) \sim 1.4$, 4, and 5 MeV respectively in the low-, medium-, and high- P_{ICRH} phases, and consequently heating mostly the electron population (the combined NBI blips and ICRH ion heating remains one order of magnitude lower than electron heating as shown in Fig. 5). That resulted in a clear increase in the electron temperature. Unexpectedly, the deepcore ion temperature was also shown to increase, which could not be explained by means of electron-ion collisional coupling or by linear effects of the energetic particles on the linear ITG microinstability [4]. The global

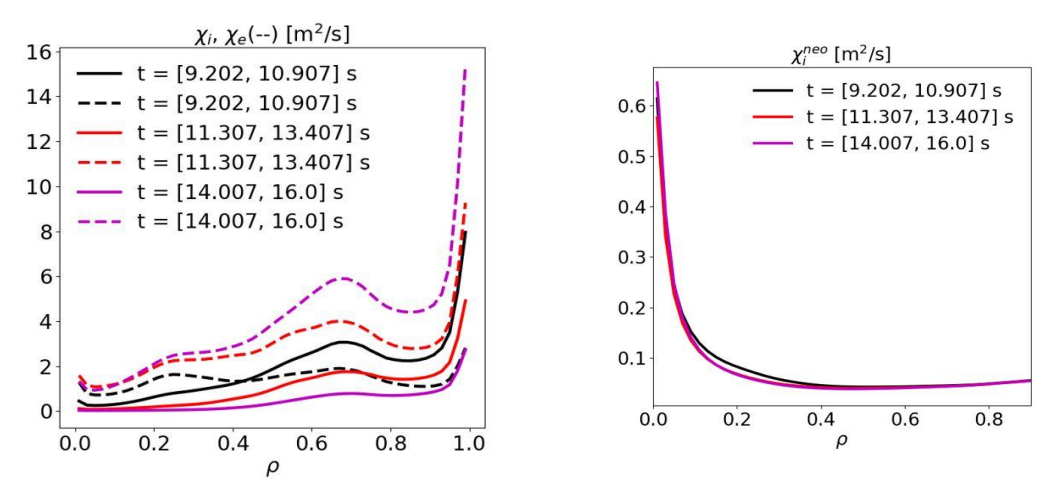


Figure 6: (left panel) Power balance analysis for the three ICRH heated phases of #97090 from low (2 MW, t=[9.2 10.9] s) to high (7 MW, t=[14 16] s) ICRH heating. (right panel) Neoclassical ion heat diffusivity radial profile.

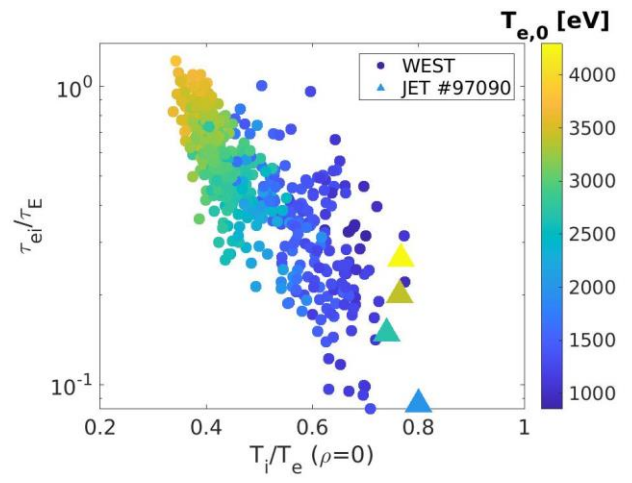


Figure 7: Collisional energy exchange time between electrons and ions over the global energy confinement time versus the central ion to electron temperature ratio for dominant electron heated WEST plasmas. JET cases with the formation of an ITB are also shown, from the ohmic phase to the 7 MW ICRH heated phase.

energy confinement for the L-mode H89P experienced a slight decrease from the Ohmic to the low- P_{ICRH} phase, but increased from the low- to the high-P_{ICRH} phase with a formation of an ITB. This improvement in confinement was attributed experimentally [4] to the presence of a zerofrequency zonal flow that was nonlinearly generated by the unstable Alfvénic modes driven by the energetic ³He in this discharge. The presence of dominant electron heating, MeV energetic particles, and the absence of rotation (no neutral beam injection was used in the plasma for heating purposes) makes this plasma a suitable candidate for studying burning plasma physics in JET as well as investigating means of maximising the central ion temperature via local turbulence stabilisation in contrast to global mechanisms observed from the WEST data analysis and modelling (Fig. 7). Indeed, the global trend of T_i/T_e with τ_{ei}/τ_E is broken in

the sense that τ_{ei}/τ_E increases (less efficient collisional heat exchange between electrons and ions) for constant T_i/T_e with increased T_i and T_e . This goes together with a decreased in ion heat diffusivities down to neoclassical levels (Fig. 6) while the electron heat diffusivity is increased (power balance analysis). Yet, uncertainties on the electron heat transport levels exist due to the fact that all the heating is assumed to be deposited on the electrons, while a substantial fraction could be lost in the presence of the unstable Alfvén eigenmodes and resulting fast ion transport.

4. SATURATION MAINTAINED EVEN IN PRESENCE OF ITB IN LOW DENSITY JET AND TORE SUPRA LHCD HEATED PLASMAS

To investigate if turbulence stabilisation alone can mitigate the central ion temperature saturation in pure electron heated plasmas, JET and Tore Supra pulses are analysed featuring central ITBs following safety factor

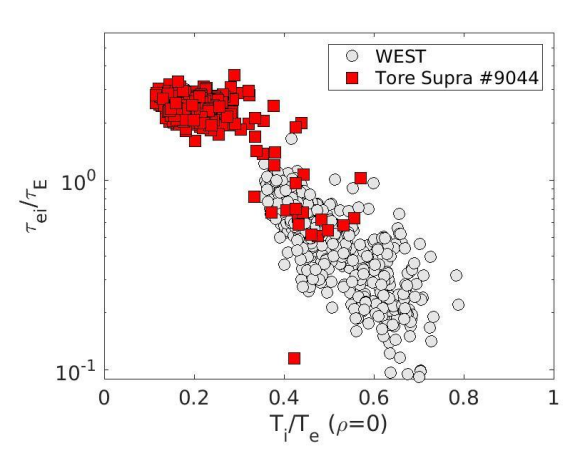


Figure 8: Data from Tore Supra during an ITB formation with LHCD heating only. The ion temperature is set to 1.6 keV as measured from charge exchange spectroscopy [12] during the ITB.

temperature (measured by charge exchange spectroscopy and consistent with the ion temperature inference from the global neutron rate) is only mildly increased (~100 eV) when the ITB is formed. This is pictured in Fig. 8 where the central ion temperature is fixed to 1.6 keV for

reversal [10-13]. Additionally, these were obtained at low densities (central electron density between 1.5 and $2.5 \times 10^{19} m^{-3}$) which provides weak ion-electron collisional coupling. Looking at Tore Supra discharge #9044, analysed in detail in [12] and clearly showing core turbulence stabilisation, the central ion

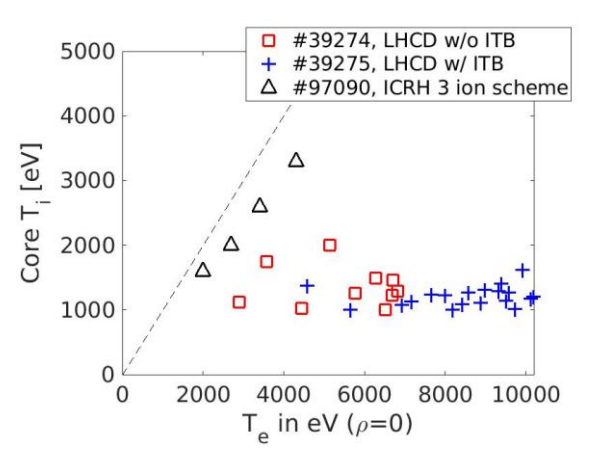


Figure 9: JET LHCD heated plasmas with and without the formation of an internal transport barrier. This is compared to the higher density ICRH heated plasma described in section 3.2.

the whole LHCD phase including the ITB formation. Compared to WEST data this perfectly fits in the trend of decreased T_i/T_e at weak collisional ion-electron coupling (large τ_{ei}/τ_E). Very similar trends are found in JET with the same ITB formations in LHCD heated pulses only at low densities [11, 13]. It has to be mentioned that for these case, the ion temperature measurements are obtained from X-ray spectroscopy at radial position $\rho \sim 0.35$. These are compared to central ion temperature measurements for the ICRH heated case (pulse #97090) obtained from charge exchange spectroscopy in Fig. 9 where the core ion temperatures are shown against the central electron temperatures. A clear saturation of T_i is found, in particular in the case of the ITB formation with negative magnetic shear, where the electron temperature increases up to 10 keV. In comparison, the ICRH heated cases, presented in section 3.2, feature increase of both T_e and T_i , with a higher core density and a reduction of the ion heat transport only. These differences and their impact on the ion temperature saturation are investigated in the following.

5. QUALITATIVE IMPACT OF THE COLLISIONAL HEAT EXCHANGE AND ION TO ELECTRON HEAT TRANSPORT

In this section, integrated modelling with METIS and the QLKNN-10D neural network for turbulent transport computations, is used to qualitatively evaluate the impact of density/collisionality on electron to ion heat exchange versus turbulent transport reduction. The neoclassical ion heat diffusivity is analytically provided using Chang-Hinton formula [21]. The starting point is the same reference WEST scenario from [2]. In this case several

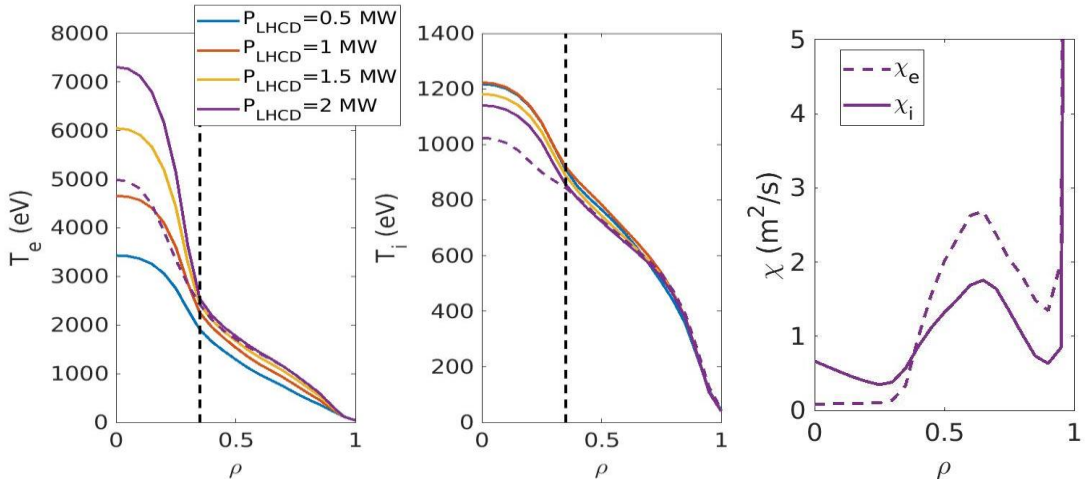


Figure 10: Electron and ion temperature profiles from METIS/QLKNN-10D steady state simulations for $\bar{n} = 2 \times 10^{19} \,\mathrm{m}^{-3}$ and increasing level of LHCD heating power. The turbulent heat diffusivities are set to 0 inside $\rho = 0.35$ (right panel). A case without turbulence stabilization at $P_{LH} = 2$ MW is shown by a dashed line.

assumptions are investigated, i.e. formation of an ad-hoc ITB inside $\rho=0.35$ by directly imposing turbulent transport to 0 (a minimum level of heat diffusivities of $0.1~m^2/s$ is still provided for numerical stability), decrease of the ion neoclassical heat diffusivity (e.g. as direct impact of lower aspect ratio A, with values for WEST of the order of 5.5 or absence of reversed q profiles) and finally turbulence stabilisation solely for the ion heat transport. The choice of the turbulence reduction from the magnetic axis to $\rho=0.35$ follows observations of reduced χ_e in Tore Supra [12] and significant increase in normalised ion temperature gradient on JET [4]. From $\rho=0.35$ up to the separatrix, the turbulent transport is not modified and taken from QLKNN-10D (flux driven). The impact of imposed turbulent transport reduction inside the ITB is pictured in Fig. 10 for $\bar{n}=2\times 10^{19}~m^{-3}$ and a scan in electron heating with LHCD. In this case, the central electron temperature increases significantly, from 5 keV to 7.2 keV with the formation of the ITB while the ion temperature increases from 1 keV to 1.2 keV with 2 MW of LHCD, despite a reduction of heat transport down to neoclassical levels (which for a WEST case can be significant with an averaged value of $\sim 0.5~m^2/s$ inside $\rho=0.35$).

To further characterise the role of density (and collisional heat exchange) in combination with transport reductions, this exercise has also been performed at higher density ($\bar{n} = 6 \times 10^{19} \, m^{-3}$). The impact of the densities and transport assumptions are all gathered in Fig. 11. The weak collisional energy exchange at low densities shows that even in the most favourable case of negligible ion heat transport (ITB combined with χ_{neo} =

0), only a mild increase in the central ion temperature is obtained. In contrast, with stronger collisional heat exchange at $\bar{n} = 6 \times 10^{19} \, m^{-3}$, the ion temperature rises up to 3.5 keV in purely electron heated plasmas and for WEST parameters (energy confinement times of the order of several 10's of ms in heated scenarios). It is worth noting that for at $\bar{n} = 6 \times 10^{19} \, m^{-3}$ and thus larger LHCD injected power to achieve relevant core T_e , a strong q reversal is observed together with enhanced neoclassical ion heat diffusivity.

When comparing to the τ_{ei}/τ_E trends, it is found that even in the case of strong ion-electron coupling and reduced ion and electron heat transport (to a minimum of $\chi=0.1~m^2/s$ inside $\rho=0.35$) there is still a significant decrease of T_i/T_e together with τ_{ei}/τ_E . This is in contradiction to the ICRH heated JET pulse shown in Fig. 7 or the nitrogen seeded WEST scenarios Fig. 4. To understand this qualitative discrepancy, the same power scan is performed for the $\bar{n}=6\times10^{19}~m^{-3}$ case with a transport barrier only on the ion heat transport. This results in qualitative agreement now with JET and WEST data, that is, an increase in τ_{ei}/τ_E at constant T_i/T_e . This is also consistent with observations of much reduced ion heat transport for the JET pulse #97090 (down to low neoclassical levels, Fig. 6) and an increase in electron heat transport inferred from power balance analysis (despite possible overestimation of the power deposition on the electrons). Thus, these simulations suggest that the most efficient way of breaking the core ion temperature saturation, for a given input electron heat transport, preventing too large increase in T_e and subsequent unfavourable reduction of collisional heat exchange.

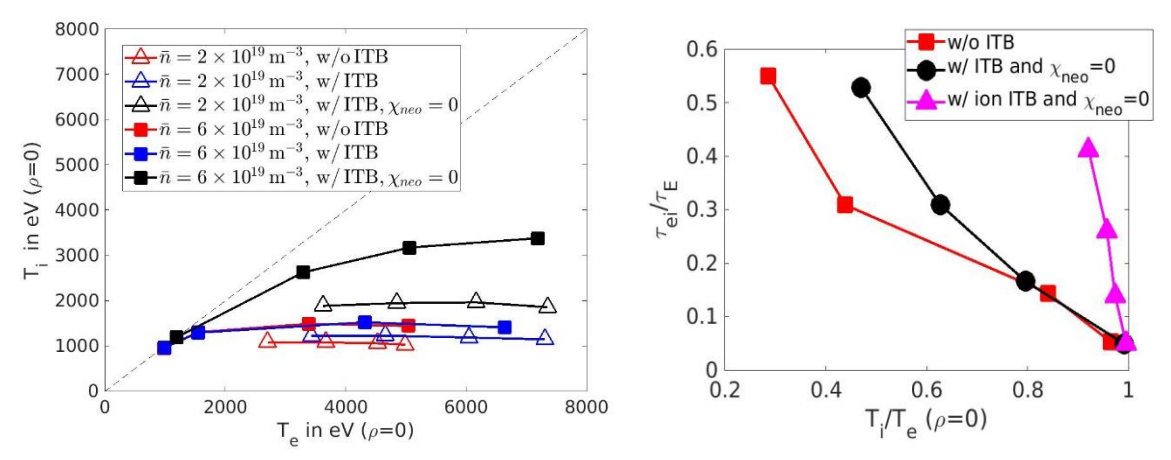


Figure 11: (left panel) Central ion versus electron temperatures for a scan in LHCD heating in different conditions, i.e. low/high densities, with/without prescribed central ITB and with/without neoclassical ion heat diffusivity. (right panel) Link between τ_{ei}/τ_{E} and the central ion to electron temperature ratio in different conditions.

6. SUMMARY AND CONCLUSIONS

The central ion temperature saturation observed in several devices, in scenarios with dominant electron heating is found to break in particular conditions, e.g. on W7-X following ITG stabilisation in pellet fuelled plasmas. In the dataset investigated in this work (JET and WEST plasmas), this breaking is characterized by an opposite global trend, of central T_i/T_e with the ion-electron collisional heat exchange time and the energy confinement time τ_{ei}/τ_E , when increasing the heating power, i.e. increasing τ_{ei}/τ_E at constant T_i/T_e . WEST nitrogen seeded plasmas featuring ion turbulence stabilisation and relatively high densities ($\bar{n} \sim 4 \times 10^{19} m^{-3}$) show significant increase in both ion and electron core temperature. Additionally, JET ICRH heated plasma (3 ion scheme with fast ions energy up to the MeV range) with reduced core ion heat transport breaks as well the ion saturation despite dominant electron heating. In contrast to these observations, ITB formations with LHCD heating only, for Tore Supra and JET in low density plasmas ($\bar{n} \sim 1.5 \times 10^{19} m^{-3}$), do not feature such increase in central T_i despite locally strong stabilisation of turbulence. Impact of basic mechanisms are investigated with integrated modelling with varying assumptions, for a WEST reference case, such as imposed reduced turbulent transport inside $\rho = 0.35$, reduced neoclassical ion heat diffusivity (e.g. changes in aspect ratios, ion-ion collisionality or cases without strong reversed q profiles), at low and high densities. Qualitative results suggest that the most efficient way of breaking the core ion temperature saturation, for a given input electron heating power, follows from a combination of high densities and reduction of ion heat transport compared to electron heat transport, preventing too large increase in T_e and subsequent unfavourable reduction of collisional heat exchange.

REFERENCES

- [1] BEURSKENS M et al, Confinement in electron heated plasmas in Wendelstein 7-X and ASDEX Upgrade; the necessity to control turbulent transport, Nuclear Fusion **61** (2021) 016015
- [2] MANAS P. et al, Maximizing the ion temperature in an electron heated plasma: from WEST towards larger devices, Nuclear Fusion **64** (2024) 036011
- [3] BEURSKENS M. et al, Ion temperature clamping in Wendelstein 7-X electron cyclotron heated plasmas, Nuclear Fusion **61** (2021) 116072
- [4] RUIZ RUIZ J. et al, Measurement of Zero-Frequency Fluctuations Generated by Coupling between Alfvén Modes in the JET Tokamak, Physical Review Letters **134**, 095103 (2025)
- [5] KAZAKOV Y. et al, On resonant ICRF absorption in three-ion component plasmas: a new promising tool for fast ion generation, Nuclear Fusion **55** (2015) 032001
- [6] VAN DE PLASSCHE K. et al, Fast modeling of turbulent transport in fusion plasmas using neural networks, Physics of Plasmas 27 (2020) 022310
- [7] ARTAUD J.F. et al, Metis: a fast integrated tokamak modelling tool for scenario design, Nuclear Fusion 58 (2018) 105001
- [8] FORD O.P. et al, Turbulence-reduced high-performance scenarios in Wendelstein 7-X, Nuclear Fusion 64 086067 (2024)
- [9] PODAVINI L., Ion-temperature- and density-gradient-driven instabilities and turbulence in Wendelstein 7-X close to the stability threshold, Journal of Plasma Physics, vol. **90**, 905900414 (2024)
- [10] PARAIL V.V et al, Predictive modelling of JET optimized shear discharges, Nuclear Fusion 39 429 (1999)
- [11] EKEDAHL A. et al, Profile control experiments in JET using off-axis lower hybrid current drive, Nuclear Fusion **38** 1397 (1998)
- [12] HOANG G.T. et al, Improved confinement in high li lower hybrid driven steady state plasmas in TORE SUPRA, Nuclear Fusion **34** 75 (1994)
- [13] LITAUDON X. et al, Electron and ion internal transport barriers in Tore Supra and JET, Plasma Physics and Controlled Fusion 41 A733 (1999)
- [14] RIVALS, N., Experiments and SOLEDGE3X modeling of dissipative divertor and X-point Radiator regimes in WEST, Nuclear Materials and Energy **40** (2024) 101723.
- [15] FONGHETTI, T., et al., WEST L-mode record long pulses guided by predictions using Integrated Modeling, Nuclear Fusion **65** (2025) 056018.
- [16] STAEBLER G.M. et al, Verification of a quasi-linear model for gyrokinetic turbulent transport, Nuclear Fusion **61** 116007 (2021)
- [17] ROMANELLI M. et al, JINTRAC: a system of codes for integrated simulation of tokamak scenarios Plasma and Fusion Research 9 3403023 (2014)
- [18] SHI S. et al, Integrated modelling of improved core plasma performance in X-Point Radiator regime on WEST, EU-US TTF Sept 12-15 2023, Nancy
- [19] BONANOMI N. et al, Effects of nitrogen seeding on core ion thermal transport in JET ILW L-mode plasmas, Nuclear Fusion 58 026028 (2018)
- [20] FABLE E. et al, High-confinement radiative L-modes in ASDEX Upgrade, Nuclear Fusion 62 024001(2022)
- [21] CHANG C.S and HINTON F.L., Effect of finite aspect ratio on the neoclassical ion thermal conductivity in the banana regime, Phys. Fluids **25** 1493–1494 (1982)